Int. J. Electrochem. Sci., 9 **(2014)** 8011 - 8023

International Journal of
ELECTROCHEMICAL
SCIENCE
www.electrochemsci.org

Synthesis of ZnO Nanoparticles Using a Zinc-Air Cell and Investigation of the Effect of Electrolyte Concentration

T.D Malevu[*], *R.O Ocaya*

University of the Free State (QwaQwa Campus), Department of Physics, P. Bag X13 Phuthaditjhaba 9866
[*]E-mail: MalevuTD@qwa.ufs.ac.za

Received: 21 August 2014 / *Accepted:* 19 September 2014 / *Published:* 28 October 2014

We propose a method to synthesize ZnO nanoparticles. A layer of well-aligned zinc oxide (ZnO) nano-needles was synthesized on zinc plate at room temperature using an environmentally friendly zinc-air cell system (ZACs). The zinc plate was the anode, and the air cathode was composed of steel wool. A porous void-paper separated the electrodes and in the presence of a low concentration NaOH electrolyte also formed the medium of transferring electrons from the anode to the cathode. In this study, the open-circuit voltage, V_{oc}, were monitored as a function of the electrolyte concentration. The electrolyte concentrations used were 0.4M, 0.5M, 0.6M, 1M and 2M. The measured values of V_{oc} were approximately 1.2V for all the five different concentrations used. The electrolyte concentration of 0.5M gave the highest V_{oc}, while 2M gave the lowest V_{oc}. The effect of concentration in orientation and length growth of the synthesized ZnO nano-needles was also studied through scanning-electron microscopy (SEM) and x-ray diffraction (XRD). It was found that the growth and orientation of ZnO nano-needles is highly dependent on the electrolyte concentration. The SEM images show good length properties of nano-needles with average sizes between 780nm and 2200nm. XRD confirms that the synthesized nano-needles are ZnO with particle sizes between 19 and 39 nm for electrolyte concentrations of 0.6M, 1M, and 2M. Crystalline forms of ZnO were observed for concentrations higher than 0.5M, but at and below 0.5M amorphous forms were observed.

Keywords: Zinc Oxide, Nano-needles, Zinc air system, Power

1. INTRODUCTION

Zinc oxide (ZnO) is one of the mostly widely studied metal oxides due to its unique properties at the nanoscale. ZnO represents a II–VI semiconductor compound with a wide direct-band gap of 3.37 eV [1] and an excitation binding energy of 60 meV [2]. It has three stable structures, namely cubic rocksalt, zincblende and hexagonal wurtzite (lattice parameters a = 0.325nm, c = 0.521nm) [3, 4]. The large band gap gives ZnO the advantage of higher voltage breakdown, reduced electronic

noise, ability to sustain large electric fields and higher power operation [5]. With the emergence of nanotechnology, this material has been employed in a wide range of industrial applications. For instance, it finds use as a semiconductor in electronics devices and sensors, as an ingredient in cosmetics and in biomedicine [6-12]. At present, there are a number of techniques or methods that are employed to synthesize ZnO nanomaterials. Some techniques are, for example, the chemical bath deposition (CBD) [13], simple precipitation (SPM) [14] and vapor–liquid–solid growth (VLSG) [15]. However, these techniques require good working vacuums, high temperature and generally involve complex processes. The methods are also corrosive and involve toxic gases. This article proposes and investigates the possibility of producing ZnO nanoparticles using a zinc-air cell system (ZAC). A survey of the increasing body of literature shows that the ZAC system has not been explored as a possible method of producing ZnO nanoparticles [16].

The proposed ZAC method uses a zinc plate as the anode, and an "air" electrode as the cathode. In reality, since an actual electrical contact is needed to connect the cell to an external circuit, the cathode is comprised of a steel-wire mesh. An electrolyte hydroxide solution, which can be sodium hydroxide (NaOH), potassium hydroxide (KOH) or lithium hydroxide (LiOH) surrounds the steel wire mesh and forms the medium through which electron-exchange occurs. The chemical reactions at the cathode produce oxygen which effectively becomes the "air" electrode. The oxygen gas that reacts with zinc to produce ZnO can be introduced in abundance through the electrolysis of water, or bubbled through from an oxygen tank or pumped in from atmospheric air. The use of atmospheric oxygen is promising as far as cost reduction is concerned. The implication for an environmentally friendly system is also far reaching and generally attractive. Figure 1 shows the construction of the ZACs.

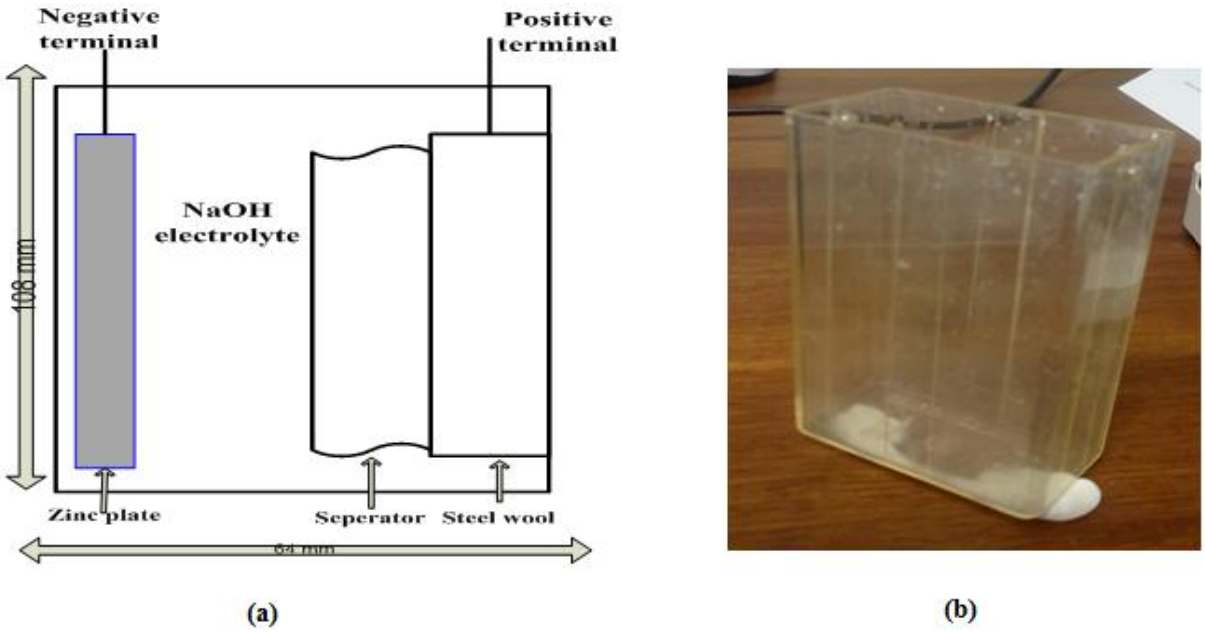

Figure 1. Typical construction of a zinc-air cell (ZAC) showing (a) schematic diagram of the layout of the ZAC (b) the perspex enclosure used for the ZAC.

2. EXPERIMENTAL

2.1. ZnO nanoparticle production using the zinc-air cell

The operation of the ZACs is described as follows: zinc loses electrons to an anode current collector and becomes a Zn^{2+} cation. The electrons generated on the anode travel via an external circuit to an air cathode where the reduction of oxygen takes place forming hydroxyl ions (OH^-). The hydroxyl ions travel towards the anode side through the electrolyte and combine with zinc cations to form ZnO. The chemical reactions of Zn–air system can be described as follows:

At positive terminal (cathode):

$$O_2 + 2H_2O + 4e^- \rightarrow 4OH^-, \quad E_{0,1} = 0.40V \tag{1}$$

At negative terminal (anode):

$$2Zn \rightarrow 2Zn^{2+} + 4e^- \tag{2}$$

$$2Zn^{2+} + 4OH^- \rightarrow 2Zn(OH)_2, \quad E_{0,2} = 1.25V \tag{3}$$

$$2Zn(OH)_2 \rightarrow 2ZnO + 2H_2O \tag{4}$$

The overall cell reaction can then be written as follow:

$$E_0 = E_{0,1} + E_{0,2}$$

$$2Zn + O_2 \rightarrow 2ZnO, \quad E_0 = 1.65V \tag{5}$$

Equation (5) permits the characterization of the ZACs open-circuit and closed-circuit behavior because the voltage output is directly measurable. With an external circuit connected, the current into a constant load can also be measured and hence the power output of the ZACs can be deduced. This allows the effect of the electrolyte on the power versus time i.e. cell energy output into a constant load to be characterized as well. In addition, the degradation of the connected cell over time can also be characterized using the deduced internal resistance. Figure 3 shows the Thevenin and Norton equivalent circuits of the cell, either of which can be used to characterize the power performance of the cell.

2.2. Fabrication of the ZACs

Solutions of pure sodium hydroxide of 0.4M to 2M concentration were prepared in distilled water using commercial sodium hydroxide pellets CP from Associated Chemical Enterprises (PTY) LTD) and distilled water. This was done by dissolving 2, 4, 6 and 8g of NaOH respectively in 100 ml distilled water under constant magnetic stirring at room temperature to ensure a homogeneously mixed solution. Then the solutions were then cooled to room temperature before being injected into the cell enclosure, Figure 1 (b). A set of zinc plates were cut into 70 mm x 50 mm plates and cleaned with steel wool until the plate appears shinny as shown in Figure 2. Copper wire was crimped onto each plate to allow external connection to the zinc anode. Commercial steel wool with the mass of 5g was used as the positive cathode. A length of copper wire was also crimped on steel wire to allow external connection to the cathode. A porous, packaging void-fill recycled paper was used to prevent a short circuit between electrodes and to allow the flow of oxygen. The zinc-plate, steel wool and void-fill paper were placed inside a clear, perspex box with the dimensions of 108 mm length, 64 mm wide and

30.4 mm width as shown in Figure 1. The oxygen from the air diffuses into the cell and it becomes the cathode reactant. The presence of the air cathode allows the reaction of oxygen and aqueous NaOH electrolyte to take place.

Figure 2. Low-resolution photograph of zinc plate after washing.

When oxygen diffuses into the electrolyte hydroxyl ions (OH-) are formed. These ions travel through the electrolyte into the zinc anode and form zinc oxide, and the chemical reactions described by Equations (1)-(5) occur.

2.3. Proposed method for ZAC system performance characterization

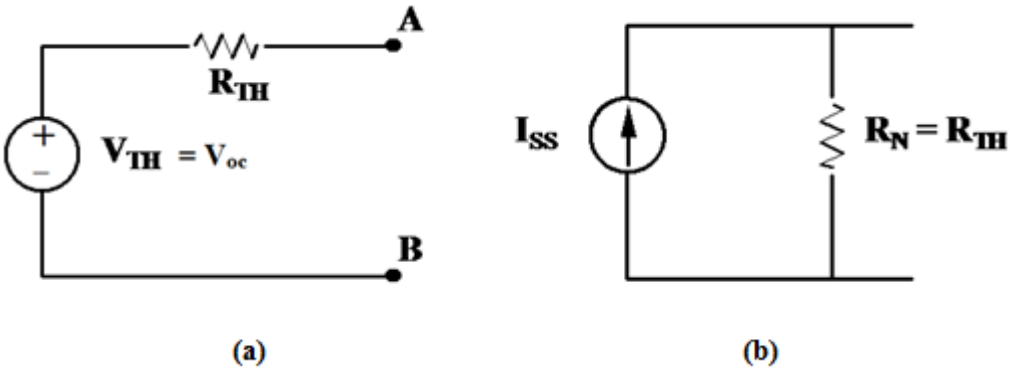

Figure 3. Equivalent circuits of the ZACs: (a) Thevenin (b) Norton.

Two multimeters were employed to evaluate the room temperature open-circuit voltage (Voc) and the constant-load, closed-circuit voltage (Vcc) performance of the ZACs. The internal resistance (Rth), current output (I) and power (P) parameters were indirectly deduced from the knowledge of Voc, Vcc and the constant load. The performance of the ZAC was then taken as the behavior of Voc, Vcc, Rth, I and P as functions of time. The closed-circuit cell load was a 470Ω/0.25 watt standard

resistor. The cell current was measured over a discharge time of 1 hour. The experiment was repeated for the five cells with the concentrations above. In order to measure V_{oc} the voltmeter was connected across point A-B in Figure 3. The current flowing through R_{th} is described using Thevenin's theorem by:

$$I_{ss} = \frac{V_{OC}}{R_{th}} \quad (6)$$

We are proposing this unique approach using standard network theory because of the following.

The infinitesimal power in a load across which a voltage drop dV is developed when a constant current I flows is given by

$$dP = IdV \quad (7)$$

The change in energy delivered to the load i.e actual work done in the load over the time interval dt is then

$$dE = dP\ dt \quad (8)$$

Assuming that the cell output is reasonably steady, the infinitesimal work done is

$$dE = P\ dt \quad (9)$$

The total energy of the cell is therefore given by

$$E = \int dE \quad (10)$$

which represents the area under the power-versus time, for example in Figure 7. This approach allows the determination of the energy delivery capacity of the cell for a specific purpose.

3. RESULTS

3.1. Open-circuit voltage behavior

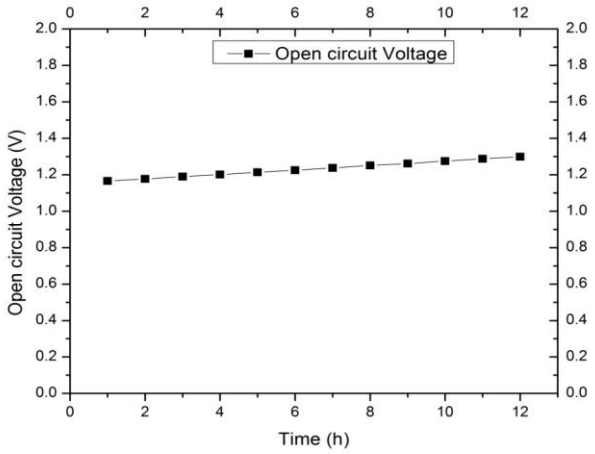

Figure 4. Twelve-hour measurements for open-circuit voltage for 2M electrolyte concentration.

Zinc air cell/batteries have theoretical and practical open-circuit voltages (V_{oc}) of 1.65V and 1.2V respectively [17, 18]. In this investigation the V_{oc} was monitored for 12 hours at room temperature and it was found to be steady at around 1.2V as shown in Figure 4. The values obtained are in agreement with Yap et al. [17] but are slightly lower than those reported by Mohamad [18]. This is due to the use of NaOH rather than KOH as the electrolyte. The specific electrolytes differ on account of the contrasting ion conductivity. However, at concentrations of 0.4, 0.6, 1 and 2M, V_{oc} is lower and the extent of passivation as a result of increased cell internal resistance is greater. The overall effect is then poorer reactions at the cathode and the anode, leading to lower power output. Overall an electrolyte concentration of 0.5M concentration was found to be the optimal concentration for ZACs open-circuit voltage, as shown in Figure 8.

3.1.1. Closed-circuit voltage characterization of the ZAC

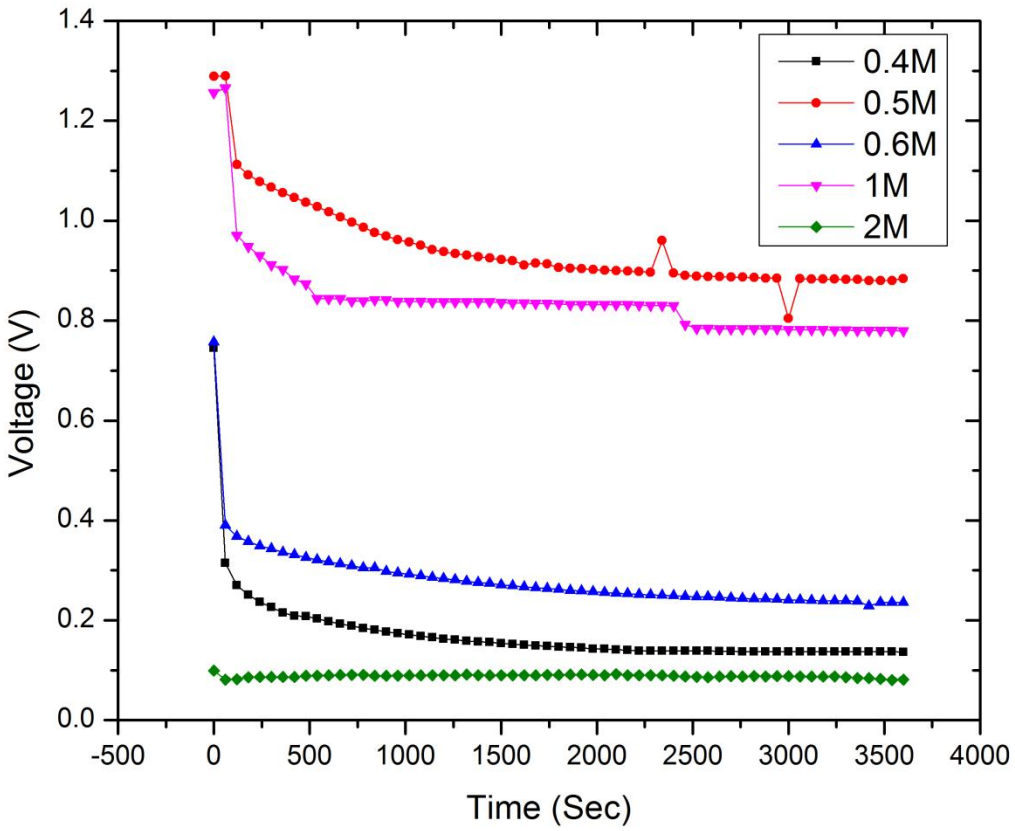

Figure 5. Open-circuit behavior of ZACs over time.

The closed-circuit voltage (Vcc) versus time performances of ZACs using electrolyte concentrations of 0.4, 0.5, 0.6, 1 and 2M over 1 hour is shown in Figure 5. The basis of our comparison was a cell voltage that remained constant within 10% of the steady-state cell output was considered to be at steady-state within the error bounds of voltage and current measurement. The graphs depict the operation of each ZAC cell under a constant 470Ω load. The graphs suggest that cells with concentrations of 0.5 and 1M can sustain steady closed-circuit voltage (V_{cc}) output longer than

those with concentrations of 0.4, 0.6, 1 and 2M. The gradual drop in the measured V_{cc} may be modeled in terms of Thevenin's theorem by including a constant voltage generator (Voc) in series with an increasing internal resistance as shown in Figure 6.

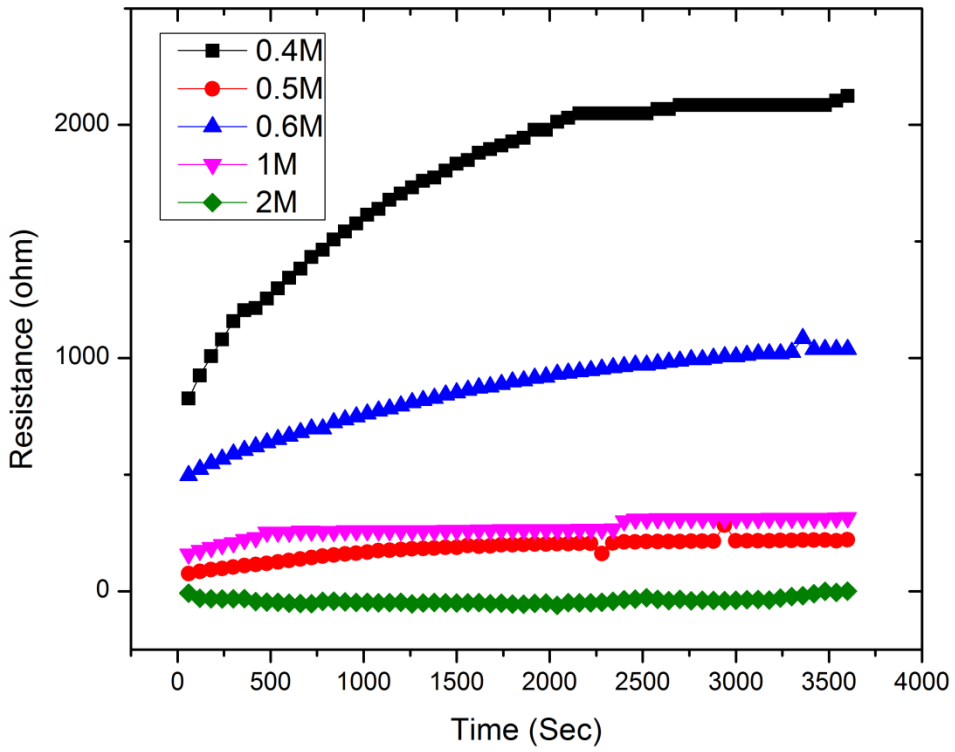

Figure 6. The variation of the internal resistance of ZACs with time.

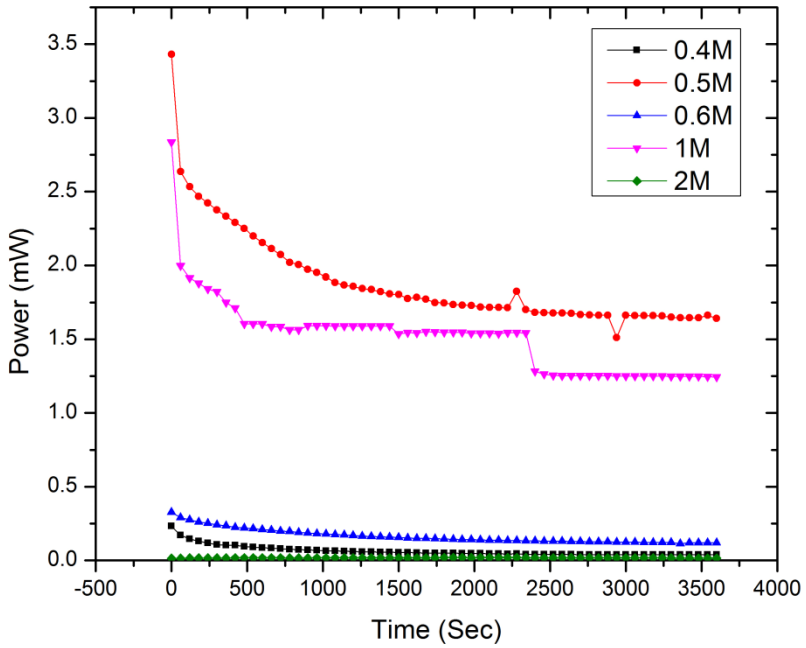

Figure 7. The deduced output energy behavior of the cells with a constant 470Ω load.

The internal resistance of the cell was measured and it is shown that the resistance of the cell depends directly on the electrolyte concentration. Figure 7 shows the output power of each ZAC as a function of time.

3.1.2. Surface morphology of the zinc electrode

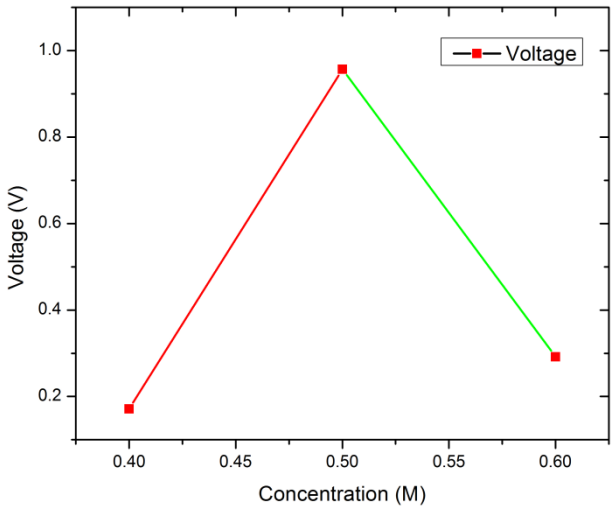

Figure 8. Optimum concentrations for ZAC system.

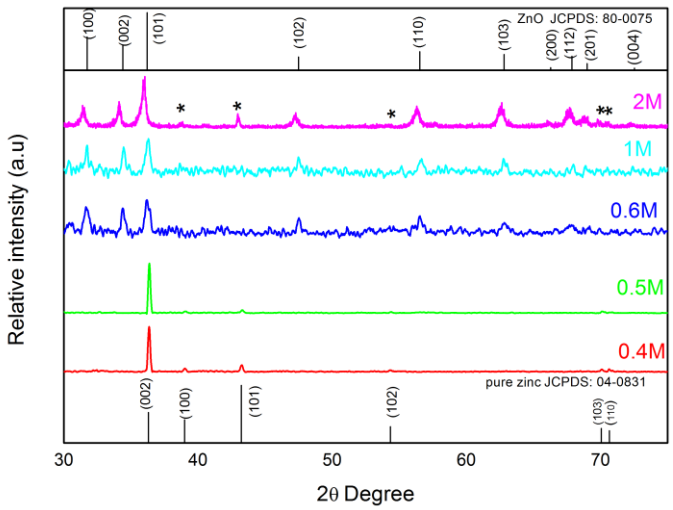

Figure 9. XRD patterns concentrations of (a) 0.4M (b) 0.5M (c) 0.6M (d) 1M and 2M.

The effects of the ZAC cell on the surface morphology of the zinc electrodes after application in the ZAC cells were then investigated by x-ray diffraction (XRD) and scanning electron microscopy (SEM). The samples for both XRD and SEM were prepared by cutting several 1cm x 1cm pieces from different parts of the zinc electrode and then repeating each measurement for each square to get a sense

of the distribution of the structures across the plate. The results of XRD for the varying electrolyte concentrations are shown in Figure 9 for electrolyte concentrations ranging from 0.4 to 2M. A comparison against standard XRD reference cards shows the presence of ZnO crystals at concentrations above 0.5M. Measurements using SEM were then carried out to determine the surface morphology of the indicated ZnO. Figure 10 shows SEM photographs at the different concentrations. The shape of the structures on the ZnO nanoparticles grown on zinc-plate is nano-needles with average particle size in the range of 19nm to 39nm. The orientation and particle sizes of these nano-needles are highly dependent on the electrolyte concentration. The higher the concentration, the more oriented the nano-needles appear to be. Figure 10 (a) shows the rough surface of the zinc plate after the synthesis at 0.4M electrolyte concentration.

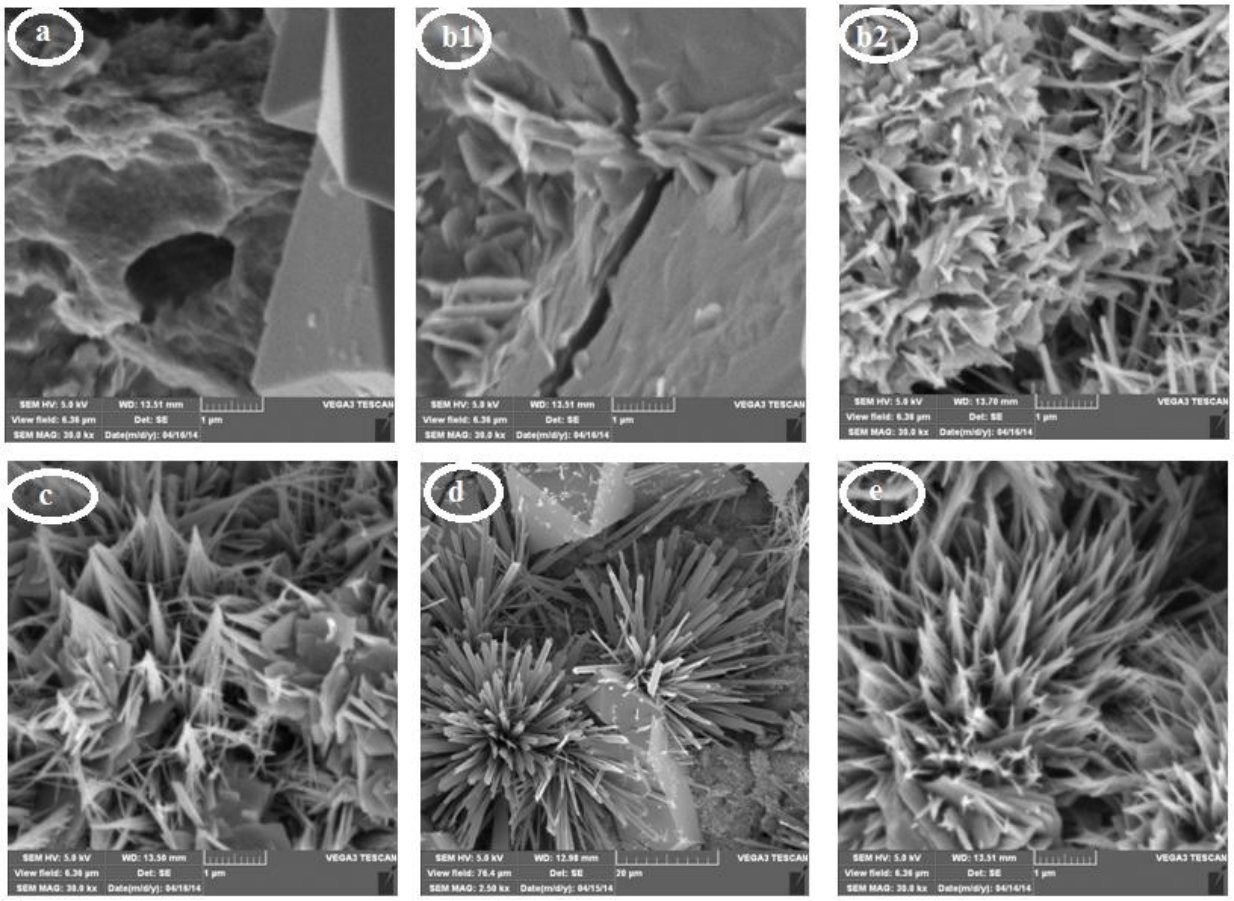

Figure 10. SEM micrographs at different electrolyte concentrations (a) 0.4M (b) 0.5M (c) 0.6M (d) 1M (e) 2M.

There is no trace of ZnO nanostructures. This can be attributed to the low formation of OH^- and low ionic conductivity of the electrolyte solution. The SEM images suggest that the formation of nano-needle structures starts at 0.5M concentration even though they are superimposed with a nano-flake-like structure. Based on these observations, different samplings were undertaken for consistency as shown in Figure 10 (b1) and (b2). From these samplings, it is apparent that during the synthesis the

current distribution on the zinc plate was not uniform. This is in agreement with the results of XRD. However, these nano-flake structures break into nano-needles with increasing concentration. This is thought to arise because the higher concentration implies a higher ionic conductivity and concentration of OH^- which then attack the rough surfaces of the nano-flakes. Figure 10 (d) shows low magnification of the ZnO nano-structure. Figure 10 (e) shows the formation of clear, sharp-tipped nano-needles. The length of the obtained nano-needles as a function of electrolyte concentration was estimated and shown in Figure 11. The average nano-needle height is in a range of 780 nm to 2200 nm, which is an indication of good properties of nano-needles [18]. Figure 11 suggests some dependence of the length of the nano-needles on electrolyte concentration for concentrations of 0.6M, 1.0M and 2.0M which are above the apparent nano-needle formation threshold 0.5M. The data appears to suggest an increasing nano-needle length with electrolyte concentration. A more detailed study of the length variation with electrolyte concentration is needed. However, Zhang et al [19] report that the morphology and size of ZnO nanorods can be tuned by adjusting the concentration of the electrolyte, the electrodeposition duration and applied current density. They observed that at fixed current density the diameters of the nanorods increased with concentration and that when the electrolyte concentration is increased from 0.5 to 1M the shapes of the self-formed ZnO structures change from cone to hexagon and attributed it to the higher growth speed of the ZnO seeds toward radial direction under higher electrolyte concentration [19]. Similar results of length dependence on electrolyte concentration were obtained by Zhu et al [20]. An XRD was employed to prove that the synthesized nanoparticles on the zinc substrate are ZnO. No characteristic peaks from impurities were observed in the samples which mean that the crystals were composed of a pure ZnO phase.

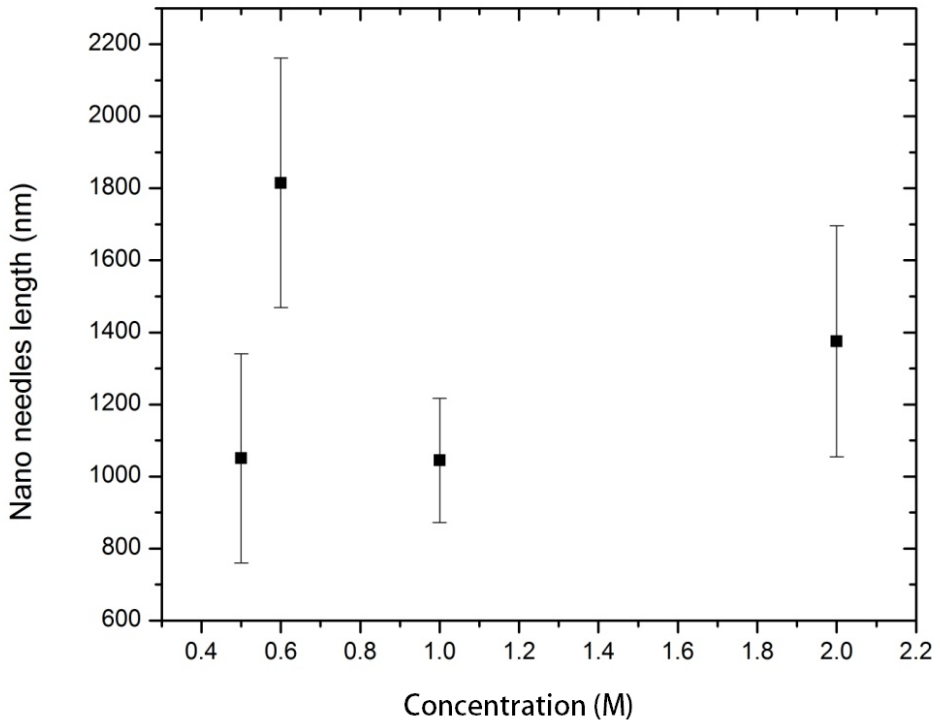

Figure 11. Estimates with error bars of the lengthwise extent of the nano-needles using SEM micrographs.

All the peaks that appears on the XRD pattern as shown in Figure 9 are in agreement with the JCPDS card number 04-0831 for hexagonal structured zinc that belongs to space group P63/mmc (194) with lattice parameters of a = 2.64 Å and c = 4.95 Å and or JCPDS card number 80-0075 for hexagonal wurtzite structured space group P63mc (186) with a maximum lattice parameter a = 3.24 Å and constant c = 5.21 Å respectively. The XRD measurements for samples synthesized at 0.4 and 0.5 M show no traces of ZnO diffraction peaks but only pure zinc diffraction peaks appears with the preferred hexagonal orientation of (002) planar. The samples prepared with 0.6M, 1M and 2M show the trademark of hexagonally wurtzite ZnO structure with preferred orientation (101). Other than the preferred orientation (101) planar, there are other 9 diffraction peaks that correspond to hexagonal wurtzite ZnO structure which are (100), (002), (102), (110), (200), (112), (201) and (004). It is also noted that as the concentration increases ZnO diffraction peaks become broad due to decrease in particle sizes. The XRD spectra show that ZnO nano-needles grown with 0.6M, 1M and 2M are crystalline. The samples prepared with 2M show some peaks that belong to pure zinc phase. This is attributed to the passivation of zinc plate due to high ionic conductivity. However, the XRD spectrum of ZnO nano-particles synthesized with 0.4M and 0.5M are the exception because they do not show any preferred significant peaks of hexagonal wurtzite ZnO structure besides the preferred (002) plane, thereby showing amorphous nature [24]. From these images, it is observed that nano-needles start to grow on a zinc plate at 0.5M with the size varying from 19 to 39nm. This is thought to be the process of effusion of atoms from the source material and these atoms rapidly lose their energy by colliding with gas atoms. The crystalline sizes of ZnO were then calculated using Debye-Scherrer equation [21].

$$D = \frac{K\lambda}{\beta \cos(\theta)} \quad (7)$$

where D is the size of the crystallites, β is the full width at half maximum of a diffraction line located at angle θ while λ is the X-ray diffraction wavelength of Cu-kα radiation (0.1514 Å) and *K* is a Scherrer constant (0.94) [21], which depends on the peak breadth, the crystallite shape, and the crystallite size distribution. The crystallite sizes varied from 19 to 39nm with increase in electrolyte concentration. The lattice spacing was calculated using Bragg's law,

$$2d\ sin\theta = n\lambda \quad (8)$$

where d is the inter-planar distance d_{hkl}, and θ is the Bragg angle (half of the peak position angle). An average lattice spacing of ~0.265 nm was obtained for the synthesized ZnO nano-needles, which can be closely correlated with the (002) interplanar spacing of ZnO wurtzite structure reported by [23]. For the wurtzite structure the inter-planar distance of the (*hkl*) plane is related to the lattice parameters *a* and *c* via the Miller indices *hkl*.

$$\left(\frac{1}{d_{hkl}}\right)^2 = \frac{4}{3} + \left(\frac{h^2+h^2+hk}{a^2}\right) + \frac{l^2}{c^2} \quad (9)$$

Where *a* and *c* are the lattice constants; *h, k, l* are Miller indices. With the approximation of the first order n =1, lattice parameter *a* was calculated using equation (10) with (002) diffraction peak:

$$a = \frac{\lambda}{\sqrt{3}\ \sin\theta} \quad (10)$$

For calculating lattice constant *c*, diffraction peak (101) and equation (11) was used

$$c = \frac{\lambda}{\sin\theta} \quad (11)$$

The application of Equations (8) to (11) to our data gives the lattice parameters shown in Table 1 for ZnO.

The calculated parameters are in agreement with the lattice parameters of the bulk ZnO. The lattice constants *a* and *c* of bulk ZnO were determined as *a* = 3.2498Å and *c* = 5.2066Å [13]. The variance in the calculated lattice constants *a* and *c* are 3.17±0.01 and 5.25±0.03, respectively. This is within the bounds of known experimental measurements [15]. However, it has been reported that the lattice parameters appear to decrease with increasing in KOH electrolyte concentration [22]. This may be due to the lattice contraction resulting from the presence of dangling bonds on the surface of the ZnO films. Further work is needed to ascertain the trend with NaOH.

Table 1. Calculated lattice parameters for wurtzite ZnO based on our experimental data.

Electrolyte concentration (M)	2θ (degrees)	Lattice constant, *c* (Å)	Lattice constant, *a* (Å)
0.4	36.350	4.94	2.85
0.5	36.36	4.94	2.85
0.6	34.453	5.23	3.21
1	34.396	5.27	3.20
2	34.189	5.29	3.10

The ions on the surface of the ZnO films are incompletely coordinated and possess unpaired electrons. These dangling bonds (Zn^{2+} and O^{2-} ions) form an electric dipole, resulting in a parallel array of dipoles originating in the boundary layer of each particle, which lies in this surface and experiences a repulsive force.

4. CONCLUSIONS

The zinc-air system has been investigated as a possible method of producing ZnO nanoparticles on a zinc plate at room temperature using a NaOH electrolyte concentration. The ZnO synthesis profile shows open-circuit voltages in a range of ~1.2V for all the five different concentrations used. The surface morphological and structural characterization confirms a layer of well-aligned crystalline (ZnO) nano-needles with the particle size varies in a range of 19nm to 39nm. The XRD spectrum shows no diffraction peaks of ZnO synthesized with 0.4M and 0.5M thus following an amorphous nature. There is some correlation between the formation of ZnO structures on the electrode, the behavior of the internal resistance and the available energy of the cell with the concentration of the NaOH electrolyte. The variation of the internal resistance of the cell under constant loading conditions is suggested as a possible tool to characterize the useful power output of the cell and its effectiveness for specific applications. Further work is needed to better quantify the effects of the formation of the nano-products and others on the electrodes with respect to the charge transfer performance of the ZAC. This is particularly important for the application of the ZAC cell to powering external devices. For

instance, it is interesting to quantify the conditions under which electrical power is maximized with regard to the formation of these products.

ACKNOWLEDGEMENT
We would like to thank Ms C. Clarke of the Department of Chemistry (UFS), for SEM characterization. It would not have been possible to carry out this research without the financial support by National Nanoscience Postgraduate Teaching and Training Platform (NNPTTP) and University of the Free State.

References

1. C. Xia, F. Wang and C. Hu, *J. Alloy Compd*, 589 (2014) 604-608
2. S. Safa, R. Sarraf-Mamoory and R. Azimirad, *Physica E Low Dimens Syst Nanostruct*, 57 (2014) 155-160
3. S. Anas, R. Metz, M.A. Sanoj, R.V. Mangalaraja and S. Ananthakumar, *Ceram Int*, 36 (2010) 2351-2358
4. V. Panchauri, K. Kern and K. Balasubramanian, *Chem Phys Lett*, 498 (2010) 317-322
5. S.S. Kumar, P. Venkateswarlu, V.R. Rao and G.N. Rao, *J. Nano Letters*, 3 (2013) 30
6. Y. Zhu and W. Shen, *J. Physica E,* 59 (2014) 110-116
7. K. Wu, J. Jiang, K. Tang, S. Gu, J. Ye, S. Zhu, L. Lu, M, Zhou, M. Xu, R. Zhang and Y. Zheng, *J. Magn Magn Mater*, 355 (2014) 51-57
8. Y. Abdi, S.M. Jebreiil-Khadem and P. Afzali, *Curr Appl Phys*, 14 (2014) 227-231
9. O. Zacharopoulou and A. Varvaresou, *Epitheorese Klinikes Farmakologias kai Farmakokinetikes*, 30 (2012) 51-54
10. A. Bhattacharya, V.P. Rao, C. Jain, A. Ghose and S. Banerjee, *Mater Lett*, 117 (2014)128-130
11. H. Huang, Q. Zhao, K. Hong and X. Huang, *Physica E Low Dimens Syst Nanostruct.,* 57 (2014) 113-117
12. J. Li, D. Guo, X. Wang, H. Wang, H. Jiang and B. Chen, *Nanoscale Res Lett,*, 5 (2010) 1063-1071
13. S. Yilmaz, *J. Supercond Nov Magn*, 27 (2014) 1083-1089.
14. T.T. Miao, D.X. Sun, Y.R, Guo, C. Li, Y. Ma, G.Z. Fang and Q.J. Pan, *Nanoscale Res Lett*, 8 (2013) 431
15. S.K. Chong, C.F. Dee and S.A. Rahman, *Nanoscale Res Lett*, 8 (2013) 1-8
16. Scopus, Citations for academic journal articles, online: http://www.scopus.com/ (2014)
17. C.K. Yap, W.C. Tan, S.S. Alias and A.A. Mohamad, *J. Alloy Compd*, 484 (2009) 934-938.
18. A.A. Mohamad, *J. Power Sources*, 159 (2006) 752-757
19. Z. Zhang, G. Meng, Q. Xu, Y. Hu, Q. Wu and Z. Hu, J. Phys. Chem. C 114 (2010) 189–193
20. Y.Q. Zhu, G.T. Fei, Y. Zhang, X.M. Chen, H.B. Tang and L.D. Zhang, J. Phys. Chem. 115 (2011) 13597–13602
21. V. Kumar, V. Kamar, S. Som, A. Yousif, N. Singh, O.M. Ntwaeaborwa, A. Kapoor and H.C. Swart, *J. Colloid Interf Sci*, 428 (2014) 8-15
22. J.P. Mathew, G. Varghese and J. Mathew, *Chinese Phys B*, 21 (2012) 078104
23. F. Ahmed, S. Kumar, N. Arshi, M.S, Anwar and R. Prakash, *Adv. Mater. Lett*, 2 (2011) 183-187
24. M. Saleem, L. Fang, A. Wakeel, M. Rashad, C.Y. Kong, *World Journal of Condensed Matter Physics*, 2 (2012) 10-15